QUARTERLY OF APPLIED MATHEMATICS
APRIL 1984

AN EXACT PARTIAL SOLUTION TO THE COMPRESSIBLE FLOW PROBLEMS OF JET FORMATION AND PENETRATION IN PLANE, STEADY FLOW*

BY

ROBERT R. KARPP

Los Alamos National Laboratory, Los Alamos

Abstract. A partial solution to the problem of the symmetric impact of two compressible fluid streams is derived. The plane, two-dimensional flow is assumed to be steady, and the inviscid, compressible fluid is of the Chaplygin (tangent gas) type. The equations governing this flow are transformed to the hodograph plane where an exact, closed-form solution for the stream function is obtained. The distribution of fluid properties along the plane of symmetry and the shape of free surface streamlines are determined by transformation back to the physical plane. The problem of a compressible fluid jet penetrating an infinite target of similar material is also solved by considering a limiting case of this solution. Differences between compressible and incompressible flows of the type considered are illustrated.

1. Introduction. The flow configuration of plane-stream impacts or the impact of a single stream upon a rigid plane boundary has significant technological applications. For example, this flow configuration explains some features associated with the bonding of metals in the explosive welding process [1]. The extremely high velocity of metallic jets produced by lined-cavity shaped charges can also be explained by examining the flow configuration of impacting streams [2]. Even the stretching of the jet has been explained by examining this flow [3].

Hydrodynamic computer codes based upon numerical techniques have solved complicated problems of jet formation, jet penetration, and explosive welding. However, the accuracy of some solutions is questionable, especially in regions of rapidly varying properties. A definite need for exact solutions to test problems involving flow configurations of practical interest exists. The exact solution to this steady-state problem may be useful for checking the accuracy of approximate solutions obtained with hydrodynamic computer codes. In addition to providing a test problem, a second purpose of this work is to better understand the effect of compressibility upon jet formation and jet penetration.

---

* Received by the editors August 6, 1982. This work was supported by the U. S. Army Armament Research and Development Command, Ballistic Research Laboratory and by the U. S. Department of Energy, Contract W-7405-Eng. 36.

The solution to the problem of impacting streams of incompressible fluids is well known. This work extends that solution to the Chaplygin type of compressible fluid.

2. Statement of the problem. The steady, symmetric interaction of two fluid streams in plane flow geometry is considered (Fig. 1 illustrates the flow configuration). The x-axis represents the plane of symmetry, and the incoming fluid streams are inclined to the x-axis by the angle α, where $0 < \alpha \leqslant \pi/2$. An inviscid, thermally nonconducting, compressible fluid with a pressure-density relation of the Chaplygin type is assumed. Far from the interaction region, the widths of the streams approach h_1, h_2, and h_3, and the incoming flow, with speed U_c, is assumed to be uniform. The pressure acting on the free surface streamlines, indicated by ψ_1, ψ_2, ψ_3, and ψ_4 in Fig. 1, is zero, and the pressure within the fluid streams far from the interaction region is also zero. According to Bernoulli's equation, the particle speed anywhere on the free surface streamlines is U_c. Conservation of mass and momentum indicates that the widths of the outgoing streams are related to the widths of the incoming streams by

$$h_2 = h_1(1 + \cos\alpha) \tag{1}$$

and

$$h_3 = h_1(1 - \cos\alpha). \tag{2}$$

Thus, the asymptotic conditions are specified, and the problem is to determine the details of the flow in the region of interaction.

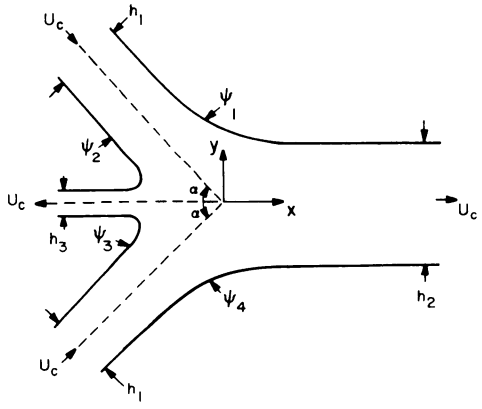

FIG. 1. Physical plane indicating symmetric impact of plane fluid streams with incoming speed U_c and impact angle α.

3. Basic equations. The equations assumed to govern plane, steady, inviscid fluid flow are

$$\frac{\partial}{\partial x}(\rho u) + \frac{\partial}{\partial y}(\rho v) = 0, \tag{3}$$

$$q\,dq + \frac{1}{\rho}dP = 0, \tag{4}$$

$$\frac{\partial u}{\partial y} - \frac{\partial v}{\partial x} = 0, \tag{5}$$

and

$$P = P(\rho), \tag{6}$$

where $q = (u^2 + v^2)^{1/2}$. In these equations, u and v denote the x- and y- components of particle velocity, q is the particle speed, ρ is the density, and P is the pressure. Eq. (3) expresses mass conservation, and Eq. (4) is Bernoulli's equation. Eq. (5) expresses the condition of irrotationality, and Eq. (6) is the pressure-density relation for the process. Eqs. (4) and (5) replace the x- and y- components of the momentum equation. This simplification is justified for inviscid flow when an equation of the form of Eq. (6) exists and when the incoming flow is irrotational. Eqs. (3) through (6) must be solved for u, v, P, and ρ as functions of x and y.

Eqs. (3) through (6) may be put into a form more convenient for analysis by introducing a velocity potential function ϕ and a stream function ψ defined by

$$\frac{\partial \phi}{\partial x} = u, \qquad \frac{\partial \phi}{\partial y} = v,$$

$$\frac{\partial \psi}{\partial x} = -\frac{\rho}{\rho_0} v, \qquad \frac{\partial \psi}{\partial y} = \frac{\rho}{\rho_0} u, \tag{7}$$

where ρ_0 is the stagnation point density. With these definitions, Eqs. (3) through (6) can be combined to form two equations for the dependent variables ϕ and ψ as functions of u and v. By introducing polar components of velocity q and θ, defined by

$$u = q \cos \theta$$

and

$$v = q \sin \theta, \tag{8}$$

the basic equations governing the flow become

$$\frac{\rho}{\rho_0} \frac{\partial \phi}{\partial \theta} = q \frac{\partial \psi}{\partial q} \tag{9}$$

and

$$\frac{\rho}{\rho_0} q \frac{\partial \phi}{\partial q} = -\left(1 - \frac{q^2}{c^2}\right) \frac{\partial \psi}{\partial \theta}, \tag{10}$$

where

$$c^2 = \frac{dp}{d\rho}. \tag{11}$$

From Eqs. (4) and (6), both the sound speed c and the density ratio ρ/ρ_0 can be expressed as functions of the particle speed q. A detailed derivation of Eqs. (9) and (10) can be found in [4]. Additional information on the derivation of these and subsequent equations is found in [5].

The equations for compressible flow, Eqs. (9) and (10), can be transformed to a form similar to the incompressible flow equations if the Chaplygin [6] pressure-density relation is used. The Chaplygin (tangent gas) relation is

$$P = P_1 - \frac{k^2}{\rho}, \tag{12}$$

where P_1 and k are constants. Equations (9) and (10) can now be written as

$$\frac{\partial \phi}{\partial \theta} = \left(1 + \frac{q^2}{c_0^2}\right)^{1/2} q \frac{\partial \psi}{\partial q} \tag{13}$$

and

$$\left(1 + \frac{q^2}{c_0^2}\right)^{1/2} q \frac{\partial \phi}{\partial q} = -\frac{\partial \psi}{\partial \theta}, \tag{14}$$

where c_0 is the sound speed at the stagnation point. A further simplification is obtained by introducing a new independent variable q_i, defined by

$$q_i = \frac{2q}{1 + \left(1 + q^2/c_0^2\right)^{1/2}}; \tag{15}$$

Eqs. (13) and (14) become

$$\frac{\partial \phi}{\partial \theta} = q_i \frac{\partial \psi}{\partial q_i}, \tag{16}$$

$$q_i \frac{\partial \phi}{\partial q_i} = -\frac{\partial \psi}{\partial \theta}. \tag{17}$$

Eqs. (16) and (17), which govern steady plane flow of a compressible fluid with a pressure-density relation given by Eq. (12), are identical to the equations governing incompressible flow if the speed variable q_i is replaced by the speed q. Thus, solution techniques appropriate to incompressible flows can now be applied. The jet formation problem is solved by obtaining a solution to Eqs. (16) and (17) that is consistent with the boundary conditions for the stated problem.

4. Boundary conditions. The stream function ψ has a constant value along any particular streamline. The mass rate of flow per unit depth $\dot{m}_{A-B}$ between any two streamlines ψ_A and ψ_B is proportional to the difference in the values of the stream function on those streamlines; that is,

$$\dot{m}_{A-B} = \rho_0(\psi_B - \psi_A). \tag{18}$$

Fig. 2 shows the free-surface streamlines ψ_1, ψ_2, ψ_3, and ψ_4 in the hodograph plane; Fig. 1 shows the physical position of these streamlines. Because the stream function is determined only to within an arbitrary constant, the value of ψ_1 will be taken as zero. The remaining values of ψ along the free-surface streamlines are determined from Eq. (18) with due account taken of the flow direction. These values are

$$\psi_1 = 0,$$
$$\psi_2 = -U_c h_1 \rho_\infty / \rho_0,$$
$$\psi_3 = -U_c(h_1 - h_3)\rho_\infty / \rho_0,$$

and

$$\psi_4 = -U_c h_2 \rho_\infty / \rho_0, \tag{19}$$

where ρ_∞ is the far-field density. These relations are the boundary conditions for ψ.

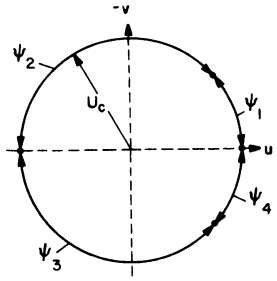

FIG. 2. Hodograph plane indicating constant values of the stream function along free-surface streamlines.

5. Solution for the complex stream function in the hodograph plane. Because the governing equations, Eqs. (16) and (17), are the Cauchy-Riemann equations in the polar coordinates $(q_i, -\theta)$, ϕ and ψ can be combined into a complex function f of a single complex variable $\bar{w}$ as

$$f(\bar{w}) = \phi(q_i, -\theta) + i\psi(q_i, -\theta), \tag{20}$$

where $\bar{w} = q_i e^{-i\theta}$. Any complex stream function f of the above form will satisfy Eqs. (16) and (17). The explicit form of the solution for f is dictated by the boundary conditions and can be computed directly from the formula of Schwarz [7]. This formula expresses the value of a complex analytic function $F(z)$ at a point z inside a circle of radius $R > |z|$, centered at $z = 0$, in terms of values of its real part on the circle. If $F(z) = U + iV$, the formula of Schwarz is

$$F(z) = \frac{1}{2\pi}\int_0^{2\pi} U(Re^{i\beta})\frac{Re^{i\beta} + z}{Re^{i\beta} - z}d\beta. \tag{21}$$

The result of applying Eq. (21) to the system represented by Eq. (20), with $F(z) = -if(z)$, is

$$\begin{aligned} -if(\bar{w}) &= \psi - i\phi \\ &= \frac{1}{2\pi}\int_0^{2\pi}\psi(U_i e^{i\beta})\frac{U_i e^{i\beta} + \bar{w}}{U_i e^{i\beta} - \bar{w}}d\beta \\ &= \frac{1}{2\pi}\left[\int_0^{\alpha}\psi_1\frac{U_i e^{i\beta} + \bar{w}}{U_i e^{i\beta} - \bar{w}}d\beta + \int_{\alpha}^{\pi}\psi_2\frac{U_i e^{i\beta} + \bar{w}}{U_i e^{i\beta} - \bar{w}}d\beta\right. \\ &\qquad \left. + \int_{\pi}^{2\pi-\alpha}\psi_3\frac{U_i e^{i\beta} + \bar{w}}{U_i e^{i\beta} - \bar{w}}d\beta + \int_{2\pi-\alpha}^{2\pi}\psi_4\frac{U_i e^{i\beta} + \bar{w}}{U_i e^{i\beta} - \bar{w}}d\beta\right], \end{aligned} \tag{22}$$

where U_i is the transformed maximum speed; that is

$$U_i = 2U_c/\left[1 + \left(1 + U_c^2/c_0^2\right)^{1/2}\right], \tag{23}$$

which is obtained from Eq. (15). When the integration in Eq. (22) is performed and the boundary values of ψ are used, the complex stream function can be expressed as

$$f(\bar{w}) = \frac{\rho_\infty}{\rho_0}\frac{U_c}{\pi}\left[h_1 \ln\left(1 - \frac{\bar{w}}{U_i e^{i\alpha}}\right) + h_1 \ln\left(1 - \frac{\bar{w}}{U_i e^{-i\alpha}}\right)\right.$$
$$\left. - h_2 \ln\left(1 - \frac{\bar{w}}{U_i}\right) - h_3 \ln\left(1 + \frac{\bar{w}}{U_i}\right)\right]. \tag{24}$$

Eq. (24) is the exact solution to the stated problem. When the expression for the complex stream function is separated into real and imaginary parts, the velocity potential and stream function are given in terms of the hodograph variables q_i and θ.

6. Partial solution in the physical plane. The transformation of the solution, Eq. (24), back to the physical plane ($z = x + iy$) is accomplished by first considering the expression

$$\begin{aligned} qe^{-i\theta}\,dz &= (u - iv)\,dz \\ &= u\,dx + v\,dy - i(v\,dx - u\,dy) \\ &= \frac{\partial\phi}{\partial x}dx + \frac{\partial\phi}{\partial y}dy - i\left(-\frac{\rho_0}{\rho}\frac{\partial\psi}{\partial x}dx - \frac{\rho_0}{\rho}\frac{\partial\psi}{\partial y}dy\right) \\ &= d\phi + i\frac{\rho_0}{\rho}d\psi. \end{aligned} \tag{25}$$

If we restrict this discussion to a single, arbitrary streamline, $d\psi = 0$ along that streamline and, from Eq. (25),

$$dz = \frac{1}{q}e^{i\theta}\,d\phi. \tag{26}$$

If Eqs. (24) and (15) are combined with Eq. (26), the result can be written as

$$dz = \frac{4c_0^2 - q_i^2}{4c_0^2\bar{w}}\frac{U_c}{\pi}\frac{\rho_\infty}{\rho_0}\left(\frac{-h_1}{U_i e^{i\alpha} - \bar{w}} - \frac{h_1}{U_i e^{-i\alpha} - \bar{w}} + \frac{h_2}{U_i - \bar{w}} - \frac{h_3}{U_i + \bar{w}}\right)d\bar{w}. \tag{27}$$

Because of the term containing q_i^2, the right side of Eq. (27) is not solely a function of the complex variable $\bar{w}$. Therefore, to integrate Eq. (27), the right side must be separated into its real and imaginary parts. For simplicity, Eq. (27) can be written as

$$dz = F(q_i, \theta)\left(e^{-i\theta}dq_i - iq_i e^{-i\theta}\,d\theta\right), \tag{28}$$

where $F(q_i, \theta)$ represents the function preceding $d\bar{w}$ in Eq. (27). The relation between q_i and θ along an arbitrary streamline, a relation that must be determined to integrate Eq. (28), can be obtained in principle from Eq. (24). On any streamline, $\psi = \psi_c$ (a constant), and the imaginary part of Eq. (24) furnishes a relation between q_i and θ, namely,

$$\psi_c = \mathrm{Im}[f(\bar{w})]. \tag{29}$$

In general, solving Eq. (29) for q_i as a function of θ or vice versa is difficult algebraically. However, at this point in the analysis, the problem has been reduced to solving an ordinary differential equation, Eq. (28), with the subsidiary condition of Eq. (29). The solution can be achieved by numerical techniques. However, the case of free-surface streamlines and the case of flow along the plane of symmetry can be treated exactly.

For the case of free-surface streamlines, $q_i = U_i$ (a constant) and $dq_i = 0$. Eq. (28) then can be written as

$$dz = F(U_i, \theta)\left(-U_i e^{-i\theta}\, d\theta\right), \tag{30}$$

or, when expanded as in Eq. (27),

$$dz = -\frac{i}{\pi}\frac{\rho_\infty}{\rho_0}\left(-\frac{h_1}{e^{i\alpha} - e^{-i\theta}} - \frac{h_1}{e^{-i\alpha} - e^{-i\theta}} + \frac{h_2}{1 - e^{-i\theta}} - \frac{h_3}{1 + e^{-i\theta}}\right) d\theta. \tag{31}$$

The integrated form of Eq. (31) is

$$z - z_0 = \frac{\rho_\infty}{\pi\rho_0}\left\{h_1 e^{-i\alpha} \ln\left[e^{i(\theta+\alpha)} - 1\right] + h_1 e^{i\alpha} \ln\left[e^{i(\theta-\alpha)} - 1\right]\right.$$
$$\left. - h_2 \ln\left[e^{i\theta} - 1\right] + h_3 \ln\left[e^{i\theta} + 1\right]\right\}, \tag{32}$$

where z_0 is the constant of integration. Eq. (32) gives the shape of the free surface streamlines in terms of the parameter θ (the angle between the x-axis and the velocity vector). For example, the streamline indicated by ψ_1 in Fig. 1 is described in the physical plane by letting θ vary from $-\alpha$ to 0 in Eq. (32). Similarly, the streamline ψ_2 is described by varying θ from $-\alpha$ to $-\pi$. The integration constant z_0, for the free-surface streamline ψ_1 can be evaluated by specifying that $y \to (1/2)h_2$ as $\theta \to 0$ and that the distance between the centerline of the incoming stream and the free streamline should approach $(1/2)h_1$ as $\theta \to -\alpha$. Similarly, z_0 can be evaluated for the free-surface streamline ψ_2 by specifying that $y \to (1/2)h_3$ as $\theta \to -\pi$ and that the distance between the centerline of the incoming stream and the free streamline ψ_2 approaches $(1/2)h_1$ as $\theta \to -\alpha$. Explicit expressions for z_0 are given in the Appendix. Equation (32) with the appropriate constants determines the shape of the free-surface streamlines in the upper half of the physical plane, Im $z > 0$. The shape of the streamlines in the lower-half plane, Im $z < 0$, can be determined by symmetry, because the x-axis represents the plane of symmetry.

For flow along the plane of symmetry, Eq. (28) again can be solved exactly. In this case, θ equals either 0 or $-\pi$ depending upon whether the point of interest lies to the right or left of the stagnation point. Consider first the streamline of symmetry to the right of the stagnation point. For this streamline, $\theta = 0$ and $d\theta = 0$. Eq. (28) can be written as

$$dz = F(q_i, 0)\, dq_i$$

or

$$dz = \frac{4c_0^2 - q_i^2}{4c_0^2 q_i}\frac{U_c}{\pi}\left(-\frac{h_1}{U_i e^{i\alpha} - q_i} - \frac{h_1}{U_i e^{-i\alpha} - q_i} + \frac{h_2}{U_i - q_i} - \frac{h_3}{U_i + q_i}\right) dq_i. \tag{33}$$

The integrated form of this equation is

$$z - z_0 = \frac{U_c}{U_i}\frac{\rho_\infty}{\pi\rho_0}\left[h_1\left(e^{-i\alpha} - \frac{U_i^2 e^{i\alpha}}{4c_0^2}\right)\ln\left(e^{i\alpha} - \frac{q_i}{U_i}\right)\right.$$
$$+h_1\left(e^{i\alpha} - \frac{U_i^2 e^{-i\alpha}}{4c_0^2}\right)\ln\left(e^{-i\alpha} - \frac{q_i}{U_i}\right)$$
$$\left.-h_2\left(1 - \frac{U_i^2}{4c_0^2}\right)\ln\left(1 - \frac{q_i}{U_i}\right) + h_3\left(1 - \frac{U_i^2}{4c_0^2}\right)\ln\left(1 + \frac{q_i}{U_i}\right)\right]. \tag{34}$$

Eq. (34) relates the position coordinate to the transformed particle speed q_i for flow in the positive x-direction. The right side of Eq. (34) is real; therefore, if $y_0 = 0$, this equation relates the position along the x-axis to the particle speed. The constant x_0 in z_0 can be chosen to position the stagnation point horizontally. For the remaining portion of the streamline of symmetry where the flow is in the negative x-direction, $\theta = -\pi$, and Eq. (28) can again be integrated. The result of this integration is the same as Eq. (34) except $-q_i$ replaces q_i and a minus sign precedes the right side of the equation.

Once the speed distribution along the plane of symmetry is determined from Eqs. (34) and (15), other distributions can be obtained from Eq. (12), and (4). The relevant relationships are

$$c_\infty^2 = k^2/\rho_\infty^2,$$
$$c_0^2 = c_\infty^2 - q_\infty^2,$$
$$c^2 = c_0^2 + q^2,$$
$$\rho^2 = k^2/c^2,$$
$$P = P_1 - k^2/\rho,$$

and

$$E = E_\infty - P_1(1/\rho - 1/\rho_\infty) + 1/2k^2(1/\rho^2 - 1/\rho_\infty^2), \tag{35}$$

where E is the specific internal energy. The last relationship is derived from the energy equation $dE = -Pd(1/\rho)$. Therefore, all properties are determined along the plane of symmetry from Eqs. (34) and (35), and the shape of the free-surface streamlines is determined from Eq. (32). Because the free-surface streamlines and the property distribution along the plane of symmetry are treated separately, the relative position of the free-surface streamlines with respect to the stagnation point is not established.

7. Partial solution to the jet penetration problem. By taking a limiting case of the foregoing solution, the problem of steady-state penetration of a jet into an infinite target can also be solved. This limiting case is achieved by allowing the angle of inclination α to approach zero while holding the jet thickness h_3 constant and then reversing the flow direction. Also, the thicknesses h_1 and h_2 must approach infinity. The resulting flow configuration is shown in Fig. 3. For incompressible flow, this transition from a jet formation solution to a jet penetration solution has been discussed by Birkhoff and Zarantonello [6].

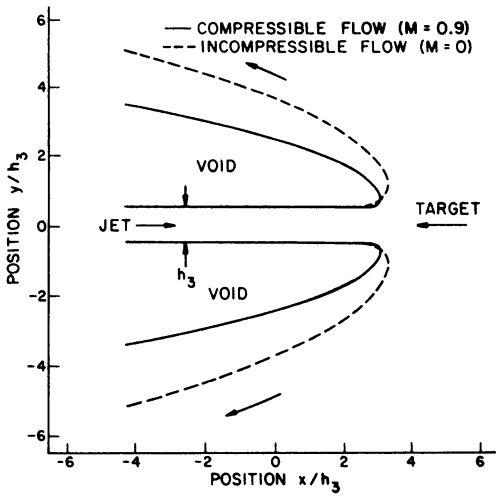

FIG. 3. Streamlines of compressible and incompressible flows for jet penetration ($\alpha \to 0°$).

In the limit as $\alpha \to 0$ with $h_3 =$ constant, the expression for the free-surface streamlines, Eq. (32), assumes the form

$$z = z_0 + \frac{\rho_\infty h_3}{\rho_0 \pi}\left[\frac{2(2 - e^{-i\theta})}{(1 - e^{-i\theta})^2} + \ln\frac{e^{i\theta} + 1}{e^{i\theta} - 1}\right]. \tag{36}$$

To insure that the thickness of the incoming flow approaches h_3 far from the stagnation point, y_0 must be computed from

$$y_0 = \frac{1}{2}h_3\left(1 - \frac{\rho_\infty}{\rho_0}\right). \tag{37}$$

The constant x_0 in z_0 merely sets the horizontal location of the streamlines. The result of applying this same limiting process to the velocity distribution formula, Eq. (34), is

$$x - x_0 = \frac{\rho_\infty h_3 U_c}{\rho_0 \pi U_i}\left\{\left(1 - \frac{U_i^2}{4c_0^2}\right)\left[\ln\frac{U_i + q_i}{U_i - q_i} + \frac{2q_i}{U_i(1 - q_i/U_i)^2}\right] + \frac{4(1 + U_i^2/4c_0^2)}{1 - q_i/U_i}\right\}. \tag{38}$$

Eq. (38) applies only to points on the plane of symmetry that are to the right of the stagnation point. For points to the left of the stagnation point, Eq. (38) applies if q_i is replaced by $-q_i$ and a minus sign is inserted before the right side of Eq. (38). As in Sec. 6, the distribution along the plane of symmetry of additional properties of the flow is determined from the relationships in Eq. (35).

8. Results and conclusion. Free-surface streamlines are shown in Figs. 3 through 5. The free-surface streamlines for jet penetration, evaluated from Eq. (36), are shown in Fig. 3. Free-surface streamlines for jet formation at impact angles of 90 and 45°, computed from

Eq. (32), are shown in Figs. 4 and 5, respectively. The values of parameters used to compute compressible flows for these and subsequent figures are

$$k^2 = 12.18 \times 10^5 GPa\, kg/m^3,$$
$$\rho_\infty = 8.9 \times 10^3 kg/m^3,$$
$$P_1 = k^2/\rho_\infty,$$
$$U_c = 3.53 km/s,$$

and

$$M = U_c/c_\infty = 0.9. \tag{39}$$

These values are appropriate for copper at low pressures, modeled as an inviscid, compressible fluid. At high pressures, the Chaplygin equation does not adequately represent copper, and the computations presented here generally overestimate the compression that would occur in a copper jet. This solution to compressible flow problems can also be used to evaluate incompressible flow by allowing $k^2 \to \infty$ in these equations. In Figs. 3 through 5, free-surface streamlines for both compressible ($M = 0.9$) and incompressible ($M = 0.0$) flow are presented. The shape of the free-surface streamline indicates that, in regions of high-streamline curvature, the curvature of streamlines of a compressible flow is greater than the curvature of streamlines of a similar incompressible flow. This

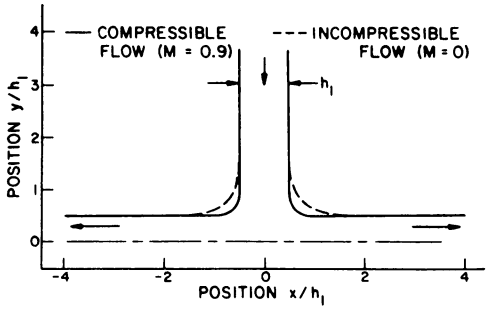

FIG. 4. Streamlines of compressible and incompressible flows for symmetric impact at normal incidence ($\alpha = 90°$).

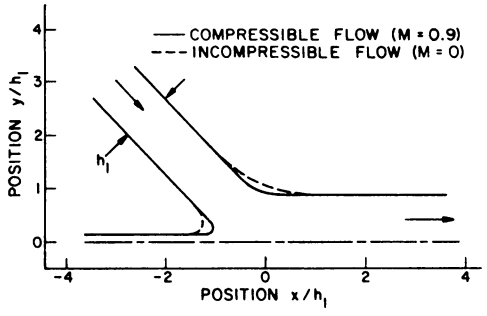

FIG. 5. Streamlines of compressible and incompressible flows for symmetric impact ($\alpha = 45°$).

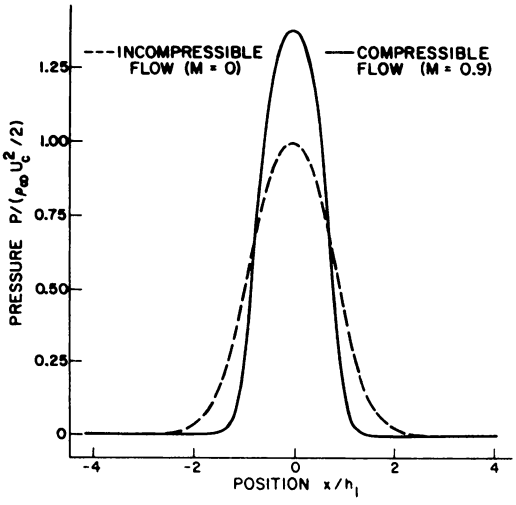

FIG. 6. Nondimensional pressure distribution along the plane of symmetry for symmetric impact at normal incidence (streamlines shown in Fig. 4).

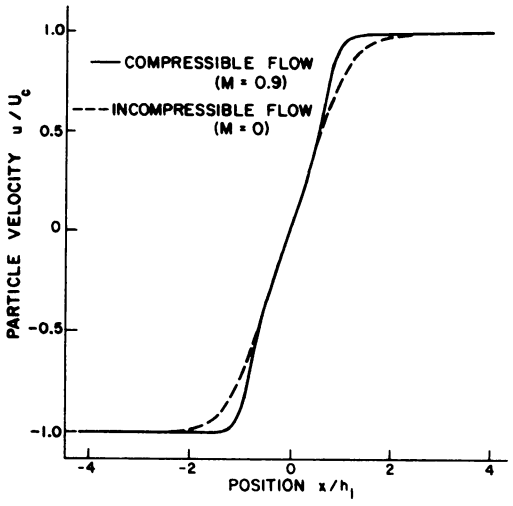

FIG. 7. Nondimensional particle velocity distribution along the plane of symmetry for symmetric impact at normal incidence (streamlines shown in Fig. 4).

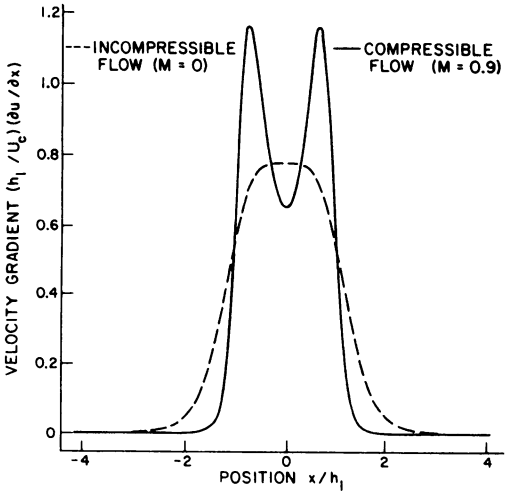

FIG. 8. Nondimensional velocity gradient distribution along the plane of symmetry impact at normal incidence (streamlines shown in Fig. 4).

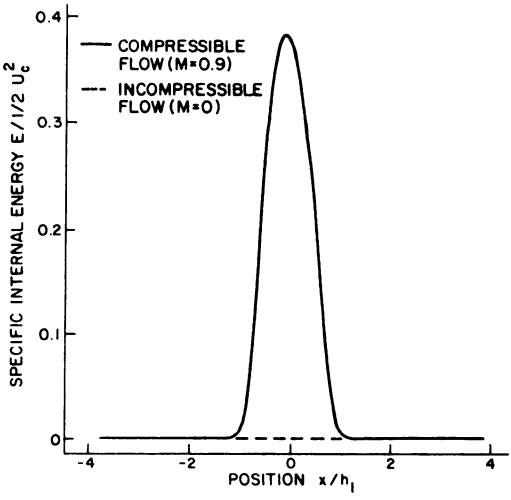

FIG. 9. Nondimensional specific internal energy distribution along the plane of symmetry for symmetric impact at normal incidence (streamlines shown in Fig. 4).

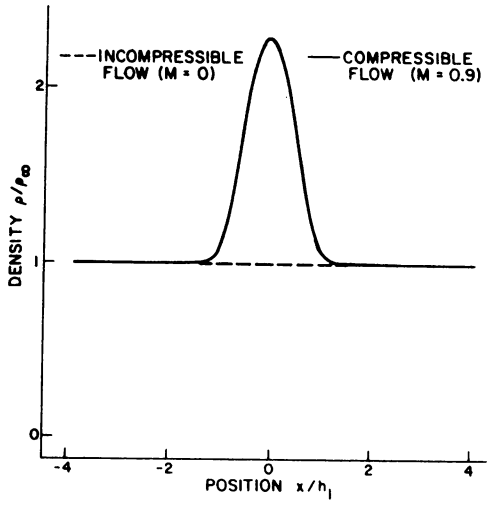

FIG. 10. Nondimensional density distribution along the plane of symmetry for symmetric impact at normal incidence (streamlines shown in Fig. 4).

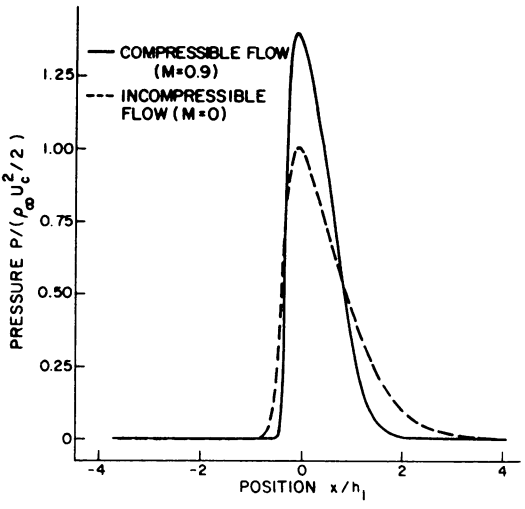

FIG. 11. Nondimensional pressure distribution along the plane of symmetry for symmetric impact at 45° (streamlines shown in Fig. 5).

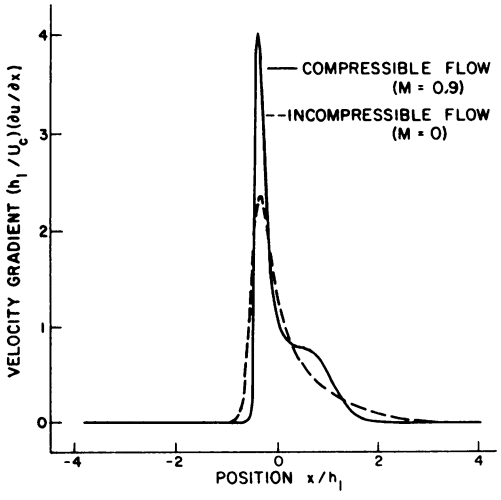

FIG. 12. Nondimensional velocity gradient distribution along the plane of symmetry for symmetric impact at 45° (streamlines shown in Fig. 5).

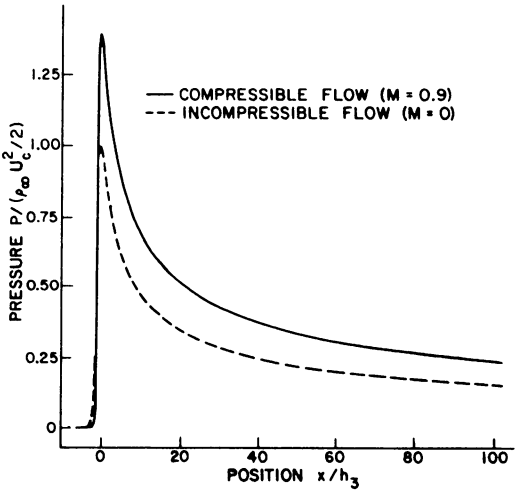

FIG. 13. Nondimensional pressure distribution along the plane of symmetry for jet penetration (streamlines shown in Fig. 3).

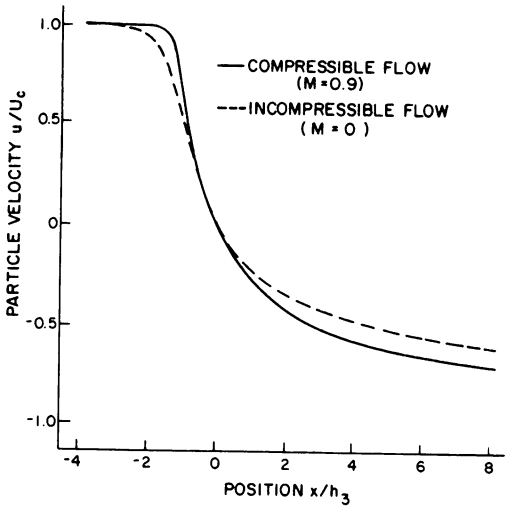

FIG. 14. Nondimensional particle velocity distribution along the plane of symmetry for jet penetration (streamlines shown in Fig. 3).

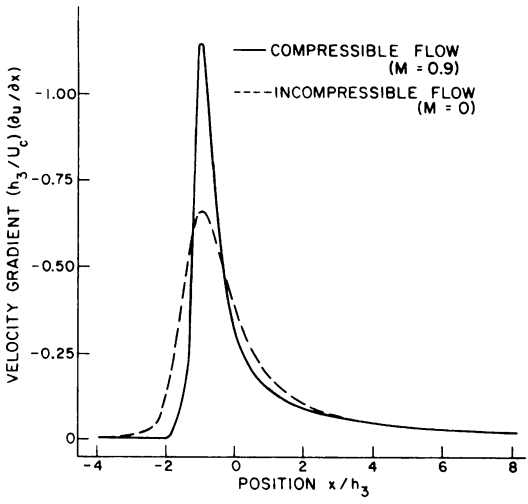

FIG. 15. Nondimensional velocity gradient distribution along the plane of symmetry for jet penetration (streamlines shown in Fig. 3).

effect is also directly evident from the factor ρ_∞/ρ_0 in Eqs. (32) and (36). The geometry of the free-surface streamlines of a compressible flow are scaled down from the free-surface streamlines of an incompressible flow.

Figs. 6 through 15 show the distribution of properties along the plane of symmetry for the flow configurations illustrated in Figs. 3 through 5. Figs. 6 through 10 give the nondimensional distributions of pressure, particle velocity, velocity gradient or strain rate ($\partial u/\partial x$), specific internal energy, and density for compressible and incompressible flows at normal incidence (Fig. 4 shows streamlines). These curves are computed from Eqs. (34) and (35). In addition to the obvious large difference in internal energy and density distributions between compressible and incompressible flows, a qualitative as well as quantitative difference exists in the velocity gradient (strain rate) as indicated by Fig. 8. For these flows, the maximum value of a property is greater for a compressible flow than for a similar incompressible flow.

Figs. 11 and 12 show the nondimensional pressure and velocity gradient distributions along the plane of symmetry for an incidence angle of 45° (Fig. 5 shows streamlines). Figs. 13 through 15 show nondimensional pressure, velocity, and velocity gradient distributions along the plane of symmetry for the jet penetration problem illustrated in Fig. 3. Fig. 13 shows the slow decrease in pressure with distance into the target. At a distance of one hundred jet thicknesses into the target from the stagnation point, the pressure is about 17% of its peak value for both compressible and incompressible flows. These flows exhibit high velocity gradients (strain rates); for example, if h_1 or h_3 equals 1.0 cm. then strain rates of the order of $10^6/s$ are found in the examples given here.

Appendix. Listed here are the explicit equations for the integration constants of Eq. (32), the equation for the shape of the free-surface streamlines. For streamline ψ_1 of Fig. 1, z_0 is given by

$$z_0 = \frac{1}{2}h_1 \csc\alpha - \frac{\rho_\infty}{\pi\rho_0}b_1 - \left[\frac{1}{2}h_2\left(1 - \frac{\rho_\infty}{\rho_0}\right) + \frac{\rho_\infty}{\pi\rho_0}a_1\right]\cot\alpha + i\frac{1}{2}h_2\left(1 - \frac{\rho_\infty}{\rho_0}\right),$$

where

$$a_1 = \frac{\pi}{2}h_1\cos\alpha + \frac{1}{2}h_1\sin\alpha\ln\left[(\cos 2\alpha - 1)^2 + \sin^2 2\alpha\right] + h_1\cos\alpha\tan^{-1}\left(\frac{-\sin 2\alpha}{\cos 2\alpha - 1}\right) - h_2\tan^{-1}\left(\frac{-\sin\alpha}{\cos\alpha - 1}\right) + h_3\tan^{-1}\left(\frac{-\sin\alpha}{\cos\alpha + 1}\right)$$

and

$$b_1 = \frac{\pi}{2}h_1\sin\alpha + \frac{1}{2}h_1\cos\alpha\ln\left[(\cos 2\alpha - 1)^2 + \sin^2 2\alpha\right] - h_1\sin\alpha\tan^{-1}\left(\frac{-\sin 2\alpha}{\cos 2\alpha - 1}\right) - \frac{1}{2}h_2\ln\left[(\cos\alpha - 1)^2 + \sin^2\alpha\right] + \frac{1}{2}h_3\ln\left[(\cos\alpha + 1)^2 + \sin^2\alpha\right]. \tag{A-1}$$

For streamline ψ_2, z_0 is given by

$$z_0 = -\frac{1}{2}h_1\csc\alpha - \frac{\rho_\infty}{\pi\rho_0}b_2 - \left[\frac{1}{2}h_3\left(1 - \frac{\rho_\infty}{\rho_0}\right) + \frac{\rho_\infty}{\pi\rho_0}a_2\right]\cot\alpha + i\frac{1}{2}h_3\left(1 - \frac{\rho_\infty}{\rho_0}\right),$$

where

$$a_2 = -\tfrac{\pi}{2}h_1\cos\alpha + \tfrac{1}{2}h_1\sin\alpha\ln\left[(\cos 2\alpha - 1)^2 + \sin^2 2\alpha\right] + h_1\cos\alpha\tan^{-1}\left(\frac{-\sin 2\alpha}{\cos 2\alpha - 1}\right) - h_2\tan^{-1}\left(\frac{-\sin\alpha}{\cos\alpha - 1}\right), + h_3\tan^{-1}\left(\frac{-\sin\alpha}{\cos\alpha + 1}\right),$$

and

$$b_2 = -\tfrac{\pi}{2}h_1\sin\alpha + \tfrac{1}{2}h_1\cos\alpha\ln\left[(\cos 2\alpha - 1)^2 + \sin^2 2\alpha\right] - h_1\sin\alpha\tan^{-1}\left(\frac{-\sin 2\alpha}{\cos 2\alpha - 1}\right) - \tfrac{1}{2}h_2\ln\left[(\cos\alpha - 1)^2 + \sin^2\alpha\right] + \tfrac{1}{2}h_3\ln\left[(\cos\alpha + 1)^2 + \sin^2\alpha\right]. \tag{A-2}$$

BIBLIOGRAPHY

[1] G. R. Cowan and A. H. Holtzman, *Flow configurations in colliding plates: explosive bonding*, J. Appl. Phys. **34**, 928–939 (1963)

[2] G. Birkhoff, D. P. MacDougall, E. M. Pugh, and G. I. Taylor, *Explosives with lined cavities*, J. Appl. Phys. **19**, 563–582 (1948)

[3] E. M. Pugh, R. J. Eichelberger, and N. Rostoker, *Theory of jet formation by charges with lined conical cavities*, J. Appl. Phys. **23**, 532–536 (1952)

[4] R. Courant and K. O. Friedrichs, *Supersonic flow and shock waves* (Interscience Publishers, Inc., New York, 1948), pp. 247–252

[5] R. R. Karpp, *An exact partial solution to the steady-state, compressible fluid flow problems of jet formation and jet penetration*, Los Alamos Scientific Laboratory report LA-8371, Los Alamos, New Mexico (October 1980)

[6] G. Birkhoff and E. H. Zarantonello, *Jets, wakes, and cavities* (Academic Press, Inc., New York, 1957), pp. 185–189

[7] L. M. Milne-Thomson, *Theoretical hydrodynamics*, 2nd Ed. (The Macmillan Co., New York, 1950), pp. 273–280